Yang *et al.*
Chinese Journal of Mechanical Engineering (2023) 36:152
https://doi.org/10.1186/s10033-023-00975-6

Chinese Journal of Mechanical Engineering

ORIGINAL ARTICLE

Open Access

Gravity-Based Kinetostatic Modeling of Parallel Manipulators Using Screw Theory

Chao Yang[1], Fengli Huang[1*], Wei Ye[2] and Qiaohong Chen[3*]

Abstract

The pose accuracy of parallel manipulators (PMs) is a key index to measure their performance. Establishing the gravity-based kinetostatic model of a parallel robot provides an important basis for its error composition and accuracy improvement. In this paper, a kinetostatic modeling approach that takes real gravity distribution into consideration is proposed to analyze the influence of gravity on the infinitesimal twist and actuator forces of PMs. First, the duality of the twist screw and constraint wrenches are used to derive the gravity-attached constraint wrenches independent of the external load and the limb stiffness matrix corresponding to the kinematics-based constraint wrenches. Second, the gravity model of the mechanism is established based on the screw theory and the principle of virtual work. Finally, the analytical formulas of the infinitesimal twist and the actuator force of PMs are obtained, and the influences of the external load, platform gravity, and rod gravity on the stiffness of the mechanism are decoupled. The non-overconstrained 3RPS and overconstrained 2PRU-UPR PMs are taken as examples to verify the proposed method. This research proposes a methodology to analyze the infinitesimal deformation of the mechanism under the influence of gravity.

Keywords Parallel manipulator, Kinetostatic model, Gravity, Screw theory

1 Introduction

Compared with the serial mechanism, the parallel manipulator (PM) has better stiffness performance, which is of great significance for the heavy-load scenario and the accuracy improvement of the robot [1, 2]. The pose accuracy of PMs is a key index to measure their performance. Establishing the gravity-based kinetostatic model of a parallel robot provides an important basis for its error composition and accuracy improvement. The kinetostatic modeling approaches [3] mainly include the finite element analysis (FEA) method, experimental method, and analytical modeling method, among which the FEA method needs to re-meshing for different configurations of the mechanism, and the calculation is time-consuming [4]. The cost of the experimental method is high and it is difficult to decouple the influence of joint clearance and component elasticity on the stiffness performance of PMs [5].

The analytical kinetostatic modeling method has become a research hotspot of PMs because of its low computational cost. It mainly includes the matrix structure displacement (MSA) method, the virtual joint method (VJM), the screw theory method, and the strain energy method. Deblaise et al. [6] established the stiffness model of the delta PM based on the MSA method, in which the deformation compatibility equation was obtained by using the principle of the total potential energy extreme value. Klimchik et al. [7] established the stiffness model of NaVaRo planar PM using the MSA

*Correspondence:
Fengli Huang
hfl@zjxu.edu.cn
Qiaohong Chen
chen_lisa@zstu.edu.cn
[1] College of Mechanical and Electrical Engineering, Jiaxing University, Jiaxing 314001, China
[2] National and Local Joint Engineering Research Center of Reliability Analysis and Testing for Mechanical and Electrical Products, Zhejiang Sci-Tech University, Hangzhou 310018, China
[3] School of Computer Science and Technology, Zhejiang Sci-Tech University, Hangzhou 310018, China

method with consideration of joint flexibility. Pashkevich et al. [8] described the link flexibility by lumped 6-DOF virtual springs and adopted VJM to establish the stiffness model of two translational DOFs of 3-PUU and 3-PRPaR PMs. Furthermore, Zhao et al. [9] proposed a stiffness modeling method by combining the VJM and MSA, and established stiffness modeling of the 3RRlS reconfigurable PM and 3(3RRlS) reconfigurable series-PMs. Hu et al. [10] proposed a stiffness modeling method based on the screw theory and basic deformation superposition principle and studied the stiffness performance of the 2-RPU+UPR overconstrained PM. Similar to the method in Ref. [10], Zhao et al. [11, 12] established the limb stiffness matrix by mapping the basic deformation to constraint wrenches and then established the stiffness modeling based on the virtual work principle and space force system equilibrium. Yan et al. [13, 14] proposed a strain energy method to establish the stiffness modeling of non-overconstrained PMs. Yang et al. [5, 15] further expanded Yan's work and proposed an elastostatic stiffness modeling approach for the overconstrained PMs based on the screw theory and strain energy.

In order to improve the accuracy of the kinetostatic model, researchers began to take the mechanism of gravity into account. Lian et al. [16, 17] established the stiffness modeling of a 5-DOF PM with the consideration of component gravity as external loads acting on the end reference point. Cervantes-Sánchez et al. [18] presented the static analysis of spatial PMs by means of the virtual work principle with consideration of the gravity of rods and moving platform as the concentrated forces acting on their center of gravity, respectively. Wang et al. [19] presented the compliance analysis of the 3-SPR PM with consideration of component gravity and joint/link compliances based on the compliance superposition. Cao et al. [20] derived the stiffness modeling of the overconstrained PMs considering gravity based on the strain energy and virtual work principle. Mei et al. [21] established the gravity compensation modeling of a five-axis PM based on the screw theory and compliance superstition principle. Zhao et al. [22] derived the deformation of a 3-DOF parallel spindle head in the gravitational field based on the VJM and screw theory, and obtained the constraint wrench caused by link gravity. However, the influence mechanism of gravity on the infinitesimal twist and actuator force was not revealed and the influence of each component's gravity on the infinitesimal twist was not decoupled in the above-mentioned methods.

The main contributions of this work are as follows: (1) the limb gravity-attached constrained wrenches independent of the external loads were proposed, and the influence of rod gravity on the actuator forces and elastic deformation corresponding to kinematics-based constrained wrenches was established; (2) a systematic kinetostatic modeling with consideration of gravity based on the screw theory, strain energy, space force system equilibrium, and virtual work principle was proposed, and the influence of component gravity on the infinitesimal twist of PMs was decoupled.

The rest of this work is structured as follows. Section 2 presents the procedure of the elastostatic stiffness modeling of PMs with consideration of gravity. The case study of a non-overconstrained PM is presented in Section 3. Section 4 introduces another case study of an overconstrained PM. Finally, the conclusions of this work are drawn in Section 5.

2 Kinetostatic Modeling of PMs with Consideration of Gravity

Figure 1 shows the schematic diagram of PMs with consideration of gravity. The moving platform is connected to the base through n chains, the fixed coordinate frame O-XYZ and the moving coordinate frame o-xyz are attached to the base and the moving platform, respectively. The assumptions of the modeling are considered as follows to facilitate the interpretation of gravity influence

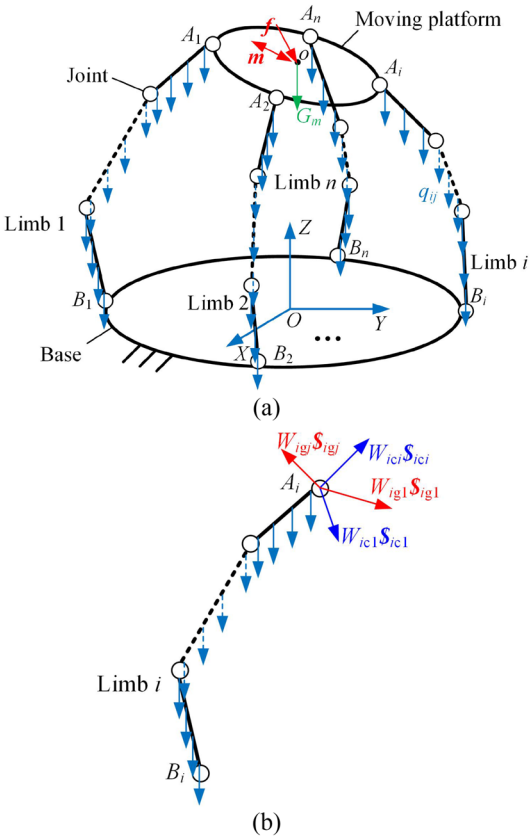

Figure 1 Schematic diagram of PM with consideration of gravity: (**a**) Force analysis of PM, (**b**) Complete constraint wrenches of the limb i

model proposed in this work: (1) Ignore the joint clearance and friction; (2) The moving platform, base, and joints are considered perfectly rigid (the static stiffness model considering joint elasticity can refer to our previous research results [5]); (3) The axial tension, shear, bending, and torsional deformation of the rods and components gravity are considered.

In this paper, the screw theory is used as the mathematical tool to establish the gravity influence model of PMs in the analytical formula. The detailed process is presented as follows.

(1) Complete limb constraint wrenches with consideration of gravity.

When the component gravity is ignored, the kinematics-based constraint wrenches of the ith limb $\boldsymbol{J}_{ic} = [\$_{ic1}, \ldots, \$_{ici}, \ldots]$ based on the kinematic analysis can be obtained by making the reciprocal product with the twist system zero, $\$_{ici}$ is the ith constraint force/couple of the ith limb with its intensity W_{ici} (Figure 1). The limb compliance/stiffness matrix corresponding to the $\boldsymbol{J}_{ic}$ can be obtained based on the strain energy and Cartesian theorem, detailed derivation can refer to Refs. [5, 15].

$$\begin{cases} \boldsymbol{C}_{ic}\boldsymbol{W}_{ic} = \boldsymbol{\Delta}_{ic}, \\ \boldsymbol{K}_{ic} = \boldsymbol{C}_{ic}^{-1}, \end{cases} \tag{1}$$

where $\boldsymbol{W}_{ic} = [W_{ic1}, \ldots, W_{ici}, \ldots]^{\mathrm{T}}$. $\boldsymbol{C}_{ic}$ and $\boldsymbol{K}_{ic}$ are the compliance and stiffness matrices corresponding to the $\boldsymbol{J}_{ic}$, respectively. $\boldsymbol{\Delta}_{ic}$ is the elastic deformation corresponding to the $\boldsymbol{J}_{ic}$.

In general, the rod gravity will do work on the twist screw and generate additional elastic deformation in the direction of the kinematics-based constraint wrenches. According to the screw theory, the work done by the kinematics-based constraint wrenches on the limb twist screw is zero.

$$W_{icj}{}^{i}\$_{icj} \circ {}^{i}\boldsymbol{S}_{ij} = 0, \tag{2}$$

where ${}^{i}\boldsymbol{S}_{ij}$ is the jth twist screw of the ith limb. The upper left symbol i indicates the vector expressed in the limb coordinate frame.

The gravity-attached constraint wrenches $\boldsymbol{J}_{ig} = [\$_{ig1}, \ldots, \$_{igk}, \ldots]$ is generated to balance the gravity; $\$_{igk}$ is the kth gravity-attached constraint wrench with its intensity is W_{igk}. According to the static equilibrium conditions of the limb, one can have

$$W_{icj}{}^{i}\$_{icj} \circ {}^{i}\boldsymbol{S}_{ij} + W_{iq}{}^{i}\$_{iq} \circ {}^{i}\boldsymbol{S}_{ij} + W_{igk}{}^{i}\$_{igk} \circ {}^{i}\boldsymbol{S}_{ij} = 0, \tag{3}$$

where ${}^{i}\$_{iq}$ is the rod gravity wrench with its intensity W_{iq}.

Combining Eqs. (2) and (3), the intensity of the gravity-attached constraint wrenches can be obtained by the property that the reciprocal product of the twist system and the constraint wrenches is zero. It is important to note that the gravity-attached constraint wrenches are independent of the external load imposed on the moving platform, and only related to the gravity of the rod. In general, the number of gravity-attached constraint wrenches is equal to the constraint degree of freedom of the joint at the connection point with the platform minus the number of kinematics-based constraint wrenches.

Accordingly, the complete limb constraint wrenches combined with kinematics-based and gravity-based constrained wrenches are given as follows:

$$\boldsymbol{J}_i = [\boldsymbol{J}_{ic1}, \ldots, \boldsymbol{J}_{ici}, \ldots \boldsymbol{J}_{ig1}, \ldots \boldsymbol{J}_{igj}, \ldots]. \tag{4}$$

(2) Kinetostatic modeling with consideration of gravity

Figure 2 shows the force diagram of the moving platform with consideration of gravity. In order to simplify the figure, only one kinematics-based constraint wrench and one gravity-attached constraint wrench are provided at each joint. The equilibrium equation of the moving platform with consideration of gravity is given by

$$\boldsymbol{W} = \sum_{i=1}^{n} \boldsymbol{J}_i \boldsymbol{W}_i = \sum_{i=1}^{n} \boldsymbol{J}_{ic} \boldsymbol{W}_{ic} + \sum_{i=1}^{n} \boldsymbol{J}_{ig} \boldsymbol{W}_{ig}, \tag{5}$$

where $\boldsymbol{W} = \boldsymbol{W}_{\mathrm{e}} + \boldsymbol{W}_{\mathrm{gm}}$, $\boldsymbol{W}_{\mathrm{e}} = [\boldsymbol{f}^{\mathrm{T}}, \boldsymbol{m}^{\mathrm{T}}]^{\mathrm{T}}$ is the external load imposed on the moving platform; $\boldsymbol{f}$ and $\boldsymbol{m}$ denote the force and couple respectively; $\boldsymbol{W}_{\mathrm{gm}}$ is the gravity load of the moving platform. $\boldsymbol{W}_i = [\boldsymbol{W}_{ic}, \boldsymbol{W}_{ig}]$, $\boldsymbol{W}_{ig} = [W_{ig1}, \ldots, W_{igj}, \ldots]^{\mathrm{T}}$.

According to the virtual work principle of the rigid moving platform, one can have

$$\boldsymbol{W}^{\mathrm{T}}\boldsymbol{\Delta} = \sum_{i=1}^{n} \boldsymbol{W}_i^{\mathrm{T}} \boldsymbol{\Delta}_i, \tag{6}$$

where $\boldsymbol{\Delta}$ is the infinitesimal twist of the point o of the moving platform. $\boldsymbol{\Delta}_i$ is elastic deformation corresponding to $\boldsymbol{W}_i$.

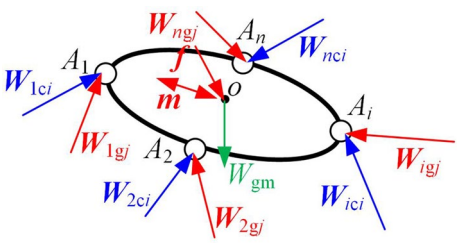

Figure 2 Force analysis diagram of the moving platform with consideration of gravity

By separating kinematics-based and gravity-based constraint wrenches, Eq. (6) can be further written as

$$\boldsymbol{W}^{\mathrm{T}}\boldsymbol{\Delta}=\sum_{i=1}^{n}\boldsymbol{W}_{ic}^{\mathrm{T}}\boldsymbol{\Delta}_{ic}+\sum_{i=1}^{n}\boldsymbol{W}_{ig}^{\mathrm{T}}\boldsymbol{\Delta}_{ig}. \tag{7}$$

Similarly, transpose Eq. (5) and multiply both sides by $\boldsymbol{\Delta}$, one can have

$$\boldsymbol{W}^{\mathrm{T}}\boldsymbol{\Delta}=\sum_{i=1}^{n}\boldsymbol{W}_{ic}^{\mathrm{T}}\boldsymbol{J}_{ic}^{\mathrm{T}}\boldsymbol{\Delta}+\sum_{i=1}^{n}\boldsymbol{W}_{ig}^{\mathrm{T}}\boldsymbol{J}_{ig}^{\mathrm{T}}\boldsymbol{\Delta}. \tag{8}$$

By comparing Eqs. (7) and (8), one can have

$$\begin{cases}\boldsymbol{\Delta}_{ic}=\boldsymbol{J}_{ic}^{\mathrm{T}}\boldsymbol{\Delta},\\ \boldsymbol{\Delta}_{ig}=\boldsymbol{J}_{ig}^{\mathrm{T}}\boldsymbol{\Delta}.\end{cases} \tag{9}$$

Accordingly, Eq. (5) can be rewritten as follows:

$$\boldsymbol{W}-\sum_{i=1}^{n}\boldsymbol{J}_{ig}\boldsymbol{W}_{ig}=\sum_{i=1}^{n}\boldsymbol{J}_{ic}\boldsymbol{K}_{ic}(\boldsymbol{\Delta}_{ic}-\boldsymbol{\Delta}_{igc}), \tag{10}$$

with

$$\boldsymbol{W}_{ic}=\boldsymbol{K}_{ic}\left(\boldsymbol{\Delta}_{ic}-\boldsymbol{\Delta}_{igc}\right), \tag{11}$$

where $\boldsymbol{\Delta}_{igc}$ is projection of the elastic deformation caused by rod gravity on the kinematics-based constraint wrenches.

Rearrange Eq. (10) lead to

$$\begin{cases}\boldsymbol{\Delta}=\boldsymbol{C}\left(\boldsymbol{W}-\sum_{i=1}^{n}\boldsymbol{J}_{ig}\boldsymbol{W}_{ig}+\sum_{i=1}^{n}\boldsymbol{J}_{ic}\boldsymbol{K}_{ic}\boldsymbol{\Delta}_{igc}\right),\\ \boldsymbol{C}=\boldsymbol{K}^{-1},\quad \boldsymbol{K}=\sum_{i=1}^{n}\boldsymbol{J}_{ic}\boldsymbol{K}_{ic}\boldsymbol{\Delta}_{ic}^{\mathrm{T}},\end{cases} \tag{12}$$

where $\boldsymbol{C}$ is the overall compliance matrix of PMs without considering the gravity, namely the inverse of the overall stiffness matrix $\boldsymbol{K}$. $\sum_{i=1}^{n}\boldsymbol{J}_{ig}\boldsymbol{W}_{ig}$ represents the influence of gravity-attached constraint wrenches on the infinitesimal twist of the moving platform. $\sum_{i=1}^{n}\boldsymbol{J}_{ic}\boldsymbol{K}_{ic}\boldsymbol{\Delta}_{igc}$ denotes the influence of the deformation along the $\boldsymbol{J}_{ic}$ caused by rod gravity on the infinitesimal twist of the moving platform. Eq. (12) not only decouples the influence of external load and component gravity on the stiffness performance of PMs, but also the influence mechanism of gravity on the stiffness performance. When the gravity influence is ignored, Eq. (12) degenerates to $\boldsymbol{\Delta}=\boldsymbol{CW}$, which is consistent with the stiffness modeling of the PMs proposed in Ref. [5].

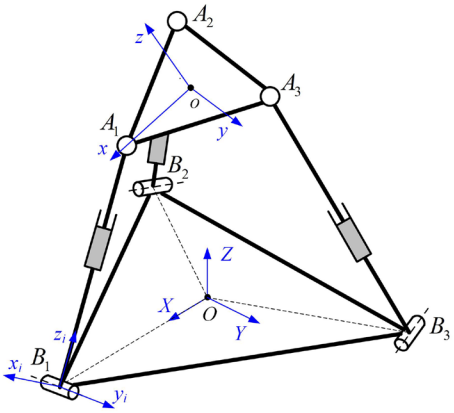

(a)

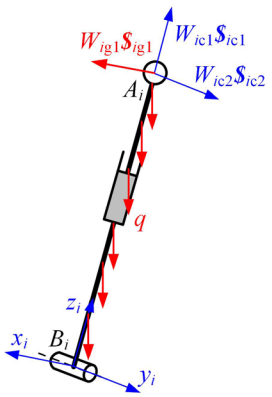

(b)

Figure 3 3RPS PM: (**a**) Schematic diagram, (**b**) Complete constrained wrenches of RPS limb with consideration of gravity

Table 1 Comparison of infinitesimal twist of point *o* of the 3RPS PM in the analytical and FEA methods

Configuration	Method	Δ_{dx}	Δ_{dy}	Δ_{dz}	Δ_{rx}	Δ_{ry}	Δ_{rz}
1	Analytical	2.435×10^{-22}	1.897×10^{-22}	-8.319×10^{-8}	1.754×10^{-22}	-2.251×10^{-22}	-2.504×10^{-21}
	FEA	1.234×10^{-19}	2.014×10^{-21}	-8.361×10^{-8}	1.881×10^{-20}	-3.158×10^{-22}	-2.138×10^{-21}
	Error (%)	–	–	0.50	–	–	–
2	Analytical	4.969×10^{-8}	5.262×10^{-8}	-7.411×10^{-8}	5.259×10^{-8}	-2.221×10^{-8}	2.590×10^{-8}
	FEA	4.972×10^{-8}	5.276×10^{-8}	-7.422×10^{-8}	5.272×10^{-8}	-2.215×10^{-8}	2.596×10^{-8}
	Error (%)	0.06	0.27	0.15	0.25	0.27	0.23

Table 2 Comparison of the intensity of constraint wrenches and actuator forces of the 3RPS PM in the analytical and FEA methods

Configuration	Method	f_{11}	f_{12}	f_{1a}	f_{21}	f_{22}	f_{2a}	f_{31}	f_{32}	f_{3a}
1	Analytical	70.855	5.418×10^{-15}	396.381	–	–	–	–	–	–
	FEA	71.136	2.144×10^{-12}	397.88	–	–	–	–	–	–
	Error (%)	0.40	–	0.38	–	–	–	–	–	–
2	Analytical	63.900	1.005	385.435	77.270	0.538	364.782	74.033	1.512	367.832
	FEA	63.483	1.003	386.220	76.863	0.535	365.450	73.625	1.506	368.520
	Error (%)	0.66	0.20	0.20	0.53	0.56	0.18	0.55	0.40	0.19

Next, two case studies that include a non-overconstrained PM and an overconstrained PM are presented to implement the proposed method in this work, wherein, two different approches are presented, one is that all the independent kinematics-based constraint wrenches act on the connection point between the limb and the moving platform, and the other is that partial independent kinematics-based constraint spirals act here.

3 Case Study 1: Non-overconstrained 3RPS PM

Figure 3 shows the 3RPS PM with three DOFs, the moving platform is connected by a spherical joint at A_i to the base by a revolute joint at B_i. The global coordinate frame and the moving coordinate frame are attached at centroid O of equilateral triangle $B_1B_2B_3$ and centroid o of equilateral triangle $A_1A_2A_3$, respectively. The X- and x-axes along OB_1 and oA_1, respectively, the Z- and z-axes are perpendicular to the base and the moving platform upward, respectively. The limb coordinate frame is attached at point B_i with its z_i- and y_i-axes point in the direction of B_iA_i and revolute axis, respectively. Structure and material parameters are designed as: radii of the base and moving platform are $r_1 = 300$ mm and $r_2 = 200$ mm, respectively, diameter of three rods is $d = 100$ mm, elasticity modulus $E = 200$ GPa, poisson ratio $\mu = 0.3$, and material density $\rho = 7820$ kg/m^3. Kinematic analysis of the mechanism can be found in Ref. [23]. The geometric constraints are defined as follows. $L_{\min} \le L_i \le L_{\max}$, L_i is the length of the rod B_iA_i, $L_{\min} = 200$ mm and $L_{\max} = 1000$ mm denote the minimum and maximum of the ith rod, respectively. $\alpha_i \le \alpha_{\max}$ with α_i and $\alpha_{\max} = 60°$ denote the angle and the maximum angle of the joints, respectively.

Based on the screw theory, the RPS limb exerts two forces on the moving platform (as shown in Figure 3(b)), one force passes through the point A_i and along the direction of the B_iA_i, and the other force passes through the point A_i and parallels to the axis of the revolute axis. The limb compliance matrix corresponding to constraint wrenches can be obtained through strain energy and Castigliano's theorem.

$$C_{ic} = \begin{bmatrix} \frac{L_i}{EA} & 0 \\ 0 & \frac{L_i}{GA} + \frac{L_i^3}{3EI} \end{bmatrix}, \tag{13}$$

where G is the shear modulus; A is the cross sectional area, and I is moment of inertia of cross-section.

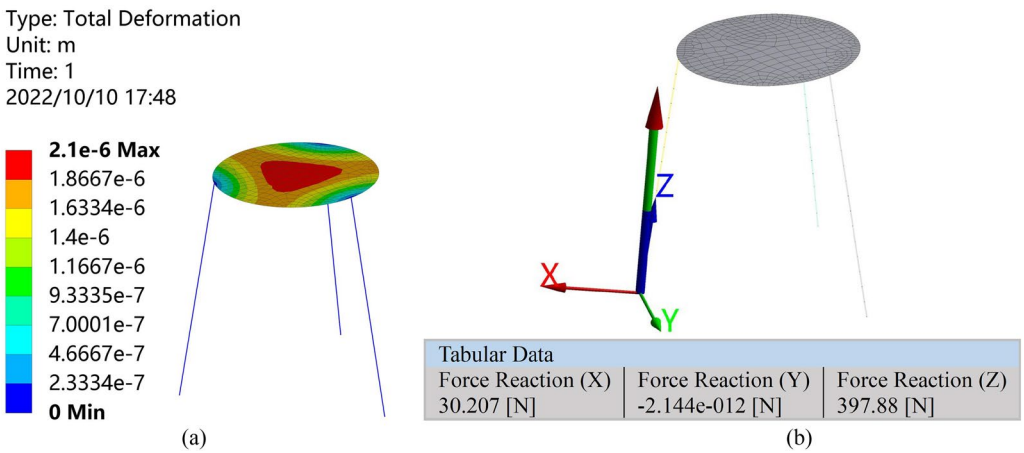

Figure 4 FEA results for the configuration 1 of the 3RPS PM: (**a**) Total deformation, (**b**) Force reaction at point B_1

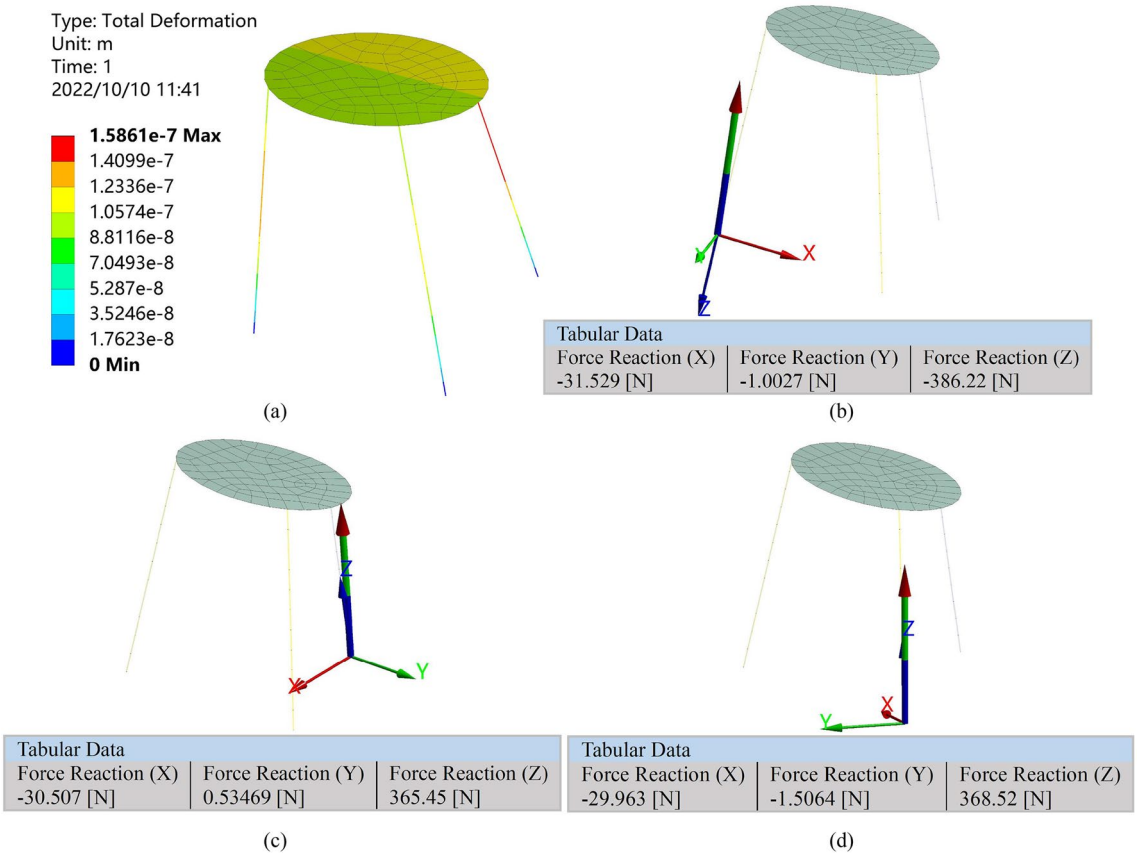

Figure 5 FEA results for the configuration 2 of the 3RPS PM: (**a**) Total deformation, (**b**) Force reaction at point B_1, (**c**) Force reaction at point B_2, (**d**) Force reaction at point B_3

As shown in Figure 3(b), the work done by the rod gravity on the revolute axis is not equal to zero except for the gravity vector along the rod axis. Based on the screw theory, it is known that the work of the kinematics-based constraint wrenches on the twist screw is zero. Therefore, a gravity-attached constraint wrench is generated to maintain the equilibrium of the rod. Since the spherical joint does not produce constraint couples, the generated gravity-attached constraint wrench is a force passing through point A_i and parallel to the x_i-axis.

According to Eq. (3), the equilibrium equation expressed in the limb coordinate frame is given as follows:

$$W_{iq}{}^{i}\$_{iq} \circ {}^{i}\boldsymbol{S}_{i1} + W_{ig1}{}^{i}\$_{ig1} \circ {}^{i}\boldsymbol{S}_{i1} = 0, \tag{14}$$

where $W_{iq} = qL_i$, ${}^{i}\$_{iq} = [\boldsymbol{e}_q, 0.5{}^{i}\boldsymbol{B}_i\boldsymbol{A}_i \times \boldsymbol{e}_q]^{\mathrm{T}}$, and $\boldsymbol{e}_q$ is the unit vector of gravity distribution; ${}^{i}\boldsymbol{S}_{i1} = [\boldsymbol{e}_2, 0, 0, 0]^{\mathrm{T}}$ is the twist screw of the revolute axis with $\boldsymbol{e}_2 = [0, 1, 0]^{\mathrm{T}}$, and ${}^{i}\$_{ig1} = [\boldsymbol{e}_1, {}^{i}\boldsymbol{B}_i\boldsymbol{A}_i \times \boldsymbol{e}_1]^{\mathrm{T}}$ with $\boldsymbol{e}_1 = [1, 0, 0]^{\mathrm{T}}$.

According to Eq. (14), W_{ig1} can be obtained as follows:

$$W_{ig1} = -0.5q_{ix}L_i, \tag{15}$$

where q_{ix} is the component of vector $\boldsymbol{q}$ on the x_i-axis.

According to the geometric constraints of the mechanism, the gravity load $\boldsymbol{q}$ has components only in the x_i- and z_i-axes. Accordingly, the elastic deformation on the direction of constraint wrenches caused by the gravity load is given by

$$\boldsymbol{\Delta}_{igc} = \left[\frac{q_{iz}L_i^2}{2EA} \quad 0 \right]^{\mathrm{T}}, \tag{16}$$

where q_{iz} is the component of gravity load $\boldsymbol{q}$ on the x_i-axis.

Accordingly, the infinitesimal twist of the point o of the moving platform can be obtained by Eq. (12), herein, $\boldsymbol{J}_{ig} = [\boldsymbol{R}_i\boldsymbol{e}_1, \boldsymbol{oA}_i \times \boldsymbol{R}_i\boldsymbol{e}_1]^{\mathrm{T}}$, $\boldsymbol{J}_{ic1} = [\boldsymbol{R}_i\boldsymbol{e}_3, \boldsymbol{oA}_i \times \boldsymbol{R}_i\boldsymbol{e}_3]^{\mathrm{T}}$, $\boldsymbol{J}_{ig} = [\boldsymbol{R}_i\boldsymbol{e}_2, \boldsymbol{oA}_i \times \boldsymbol{R}_i\boldsymbol{e}_2]^{\mathrm{T}}$, $\boldsymbol{R}_i$ is the rotation matrix from limb to global coordinate frame, and $\boldsymbol{e}_3 = [0, 0, 1]^{\mathrm{T}}$.

Furthermore, the actuation force of the ith limb to equilibrium gravity loads can be obtained as follows:

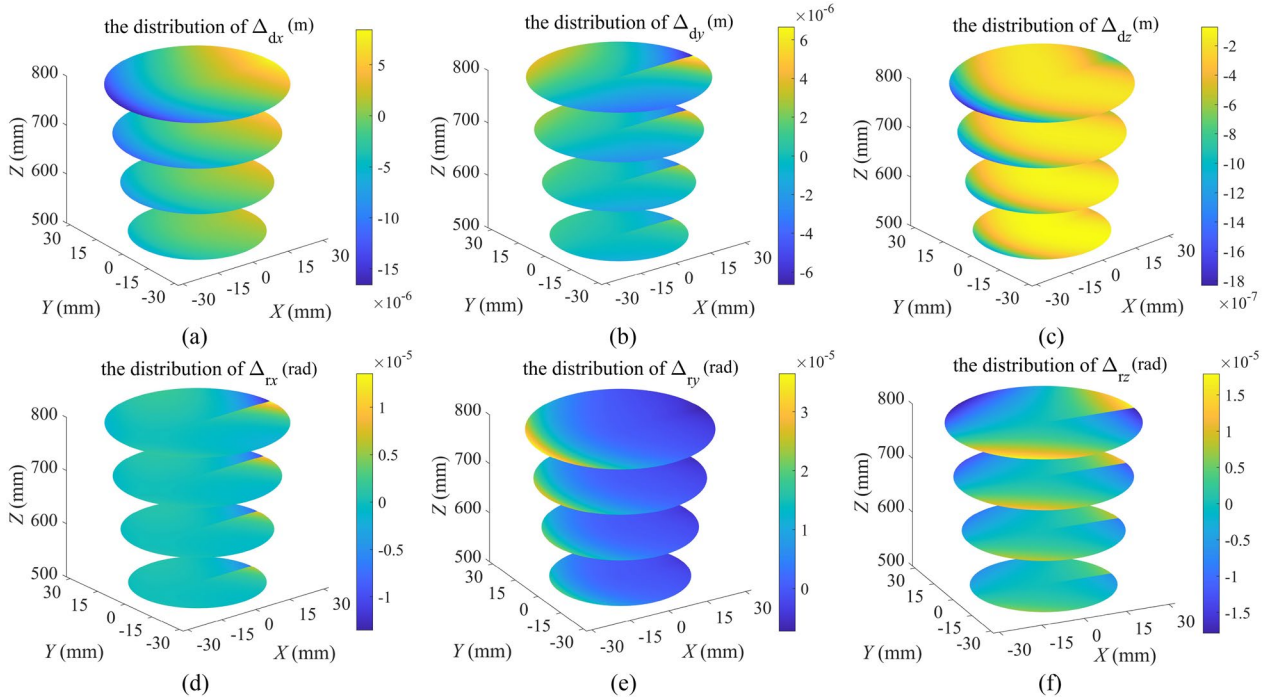

Figure 6 Infinitesimal twist of point *o* of the 3RPS PM under the influence of gravity: (**a**) Δ_{dx}, (b) Δ_{dy}, (c) Δ_{dz}, (d) Δ_{rx}, (e) Δ_{ry}, (f) Δ_{rz}.

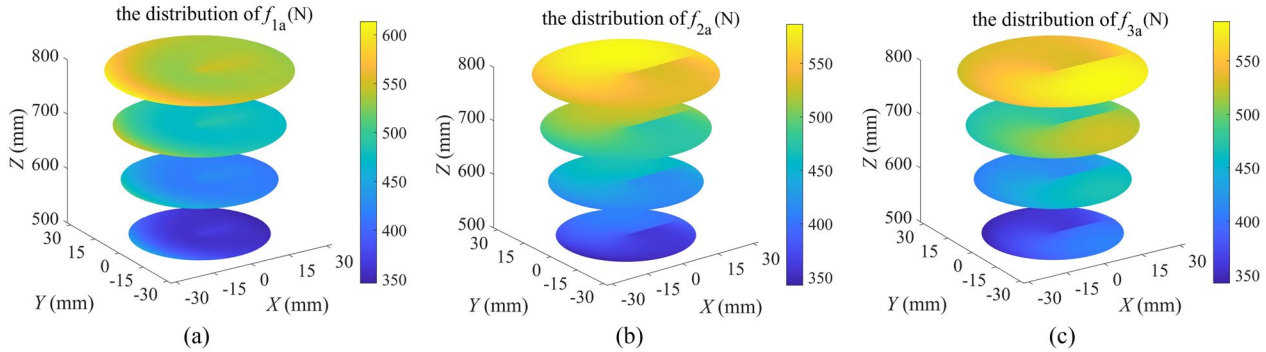

Figure 7 Actuator force of the 3RPS PM under the influence of gravity: (a) f_{1a}, (b) f_{2a}, (c) f_{3a}

$$W_{ia} = W_{ic1} + q_{iz}L_i. \tag{17}$$

Considering whether the mechanism is rationally symmetric, two configurations are selected to verify the correctness of the proposed method: configuration 1, a rotationally symmetric configuration, $L_1 = L_2 = L_3 = 550$ mm; configuration 2, an asymmetric configuration, $L_1 = 544.30$ mm, $L_2 = 488.24$ mm, and $L_3 = 498.10$ mm. Table 1 shows the comparison of the infinitesimal twist of point *o* of the 3RPS PM in the analytical and FEA methods when only gravity is considered. The maximum relative error is less than 0.5%. Table 2 shows the comparison of the intensity of constraint wrenches and actuator forces of the 3RPS PM, the maximum relative error is within 0.7%. The results show the accuracy of the kinetostatic modeling with consideration of gravity proposed in this paper. It is worth noting that due to the symmetry of the mechanism in configuration 1, only the results for limb 1 are given in Table 2. Figures 4 and 5 respectively show the FEA results of Configuration 1 and 2 of the 3RPS PM. It is noteworthy that the moving platform shown in Figure 4 is considered to be elastic with the elasticity modulus close to the rigid body to guarantee the graphics quality.

Figure 6 shows the infinitesimal twist of the point o of the 3RPS PM in the regular workspace with the gravity

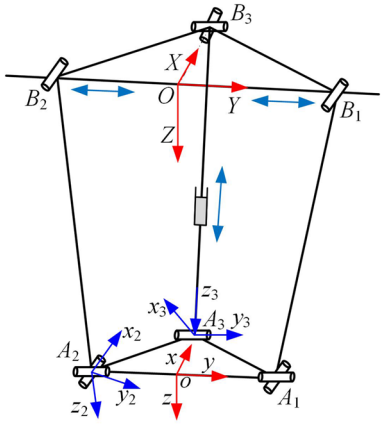

Figure 8 Schematic diagram of the 2PRU-UPR PM

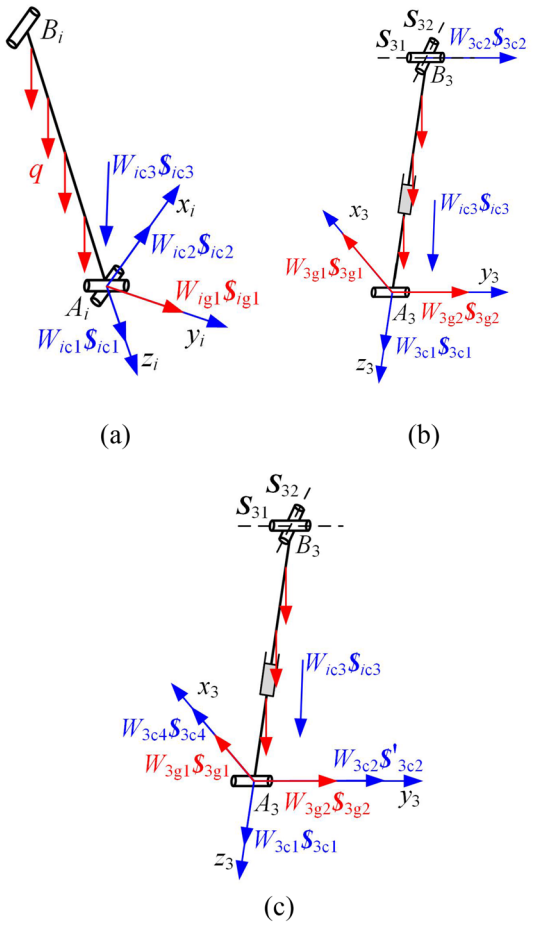

Figure 9 Complete constraint wrenches of limbs of the 2PRU-UPR PM: (**a**) PRU limbs (i = 1, 2), (**b**) UPR limb: scenario 1, (**c**) UPR limb: scenario 2

considered. The maximum linear twist is about 16 μm, and the maximum angular twist is about 0.002°. Figure 7 shows the actuator force of the mechanism with the consideration of gravity, the maximum actuator force of 600 N is required to equilibrium the gravity of the mechanism.

4 Case Study 2: Overconstrained 2PRU-UPR PM

Figure 8 shows the 3-DOF 3PRU-UPR PM, namely a translation along the line perpendicular to the two axes of the U-joint, a rotation β about the y-axis, and a rotation γ about the X-axis. The moving platform is connected to the base by two PRU limbs and one UPR limb, global coordinate frame O-XYZ, moving coordinate frame o-xyz, and limb coordinate frame A_i-$x_iy_iz_i$ are respectively attached to the base, moving platform, and ith limb. The z_i-axis along the direction of B_iA_i, x_i– (i = 1,2) and y_3-axes along the direction of the revolute axis in the ith limb. $oA_1 = oA_2 = oA_3 = r_m = 250$ mm, $OB_3 = r_b = 500$ mm, $A_1B_1 = A_2B_2 = L = 700$ mm, $OB_1 = a_1$, $OB_2 = a_2$, and $A_3B_3 = a_3$, the diameter of the links are $d = 60$ mm, material constants are the same as those of the 3RPS PM. More details about the inverse kinematics can refer to Ref. [24].

Figure 9(a) shows the complete constraint wrenches of the PRU limb. When gravity is ignored, the PRU limb exerts three constraint wrenches on the moving platform that includes a force W_{ic1} passing through the point A_i and in the direction of B_iA_i, a force W_{ic2} passing the point A_i and in the direction of the revolute axis, a couple W_{ic3} perpendicular to two axes of the universal joint. The compliance/stiffness matrix corresponding to the constraint wrenches can be found in Refs. [15, 25]. When gravity is considered, a gravity-attached force that passes through the point A_i and in the direction y_i-axis is necessary to equilibrium the work done by the gravity on the revolute axis.

According to Eq. (14), the intensity of the gravity-attached constrained wrench can be obtained as follows:

$$W_{ig1} = -0.5q_{iy}L_i, \quad (i = 1,\ 2), \tag{18}$$

where q_{iy} is the component of vector $\boldsymbol{q}$ on the y_i-axis.

According to the geometric constraints of the mechanism, the gravity load $\boldsymbol{q}$ has components only in the y_i- and z_i- axes. Accordingly, the elastic deformation on the direction of constraint wrenches caused by the gravity load is given by

$$\boldsymbol{\Delta}_{igc} = \left[\ \frac{q_{iz}L_i^2}{2EA}\ \ 0\ \ 0\ \right], \quad (i = 1,\ 2). \tag{19}$$

The UPR limb exerts a force W_{3c1} along the direction of B_3A_3, a force W_{3c2} passes through point B_3 and

Table 3 Comparison of infinitesimal twist of point *o* of the 2PRU-UPR PM in the analytical and FEA methods

Configuration	Method	Δ_{dx}	Δ_{dy}	Δ_{dz}	Δ_{rx}	Δ_{ry}	Δ_{rz}
1	Analytical	2.373×10^{-5}	0	2.633×10^{-7}	0	-3.932×10^{-5}	0
	FEA	2.380×10^{-5}	2.477×10^{-13}	2.638×10^{-7}	5.927×10^{-13}	-3.943×10^{-5}	-9.168×10^{-13}
	Error (%)	0.29	/	0.18	/	0.28	/
2	Analytical	2.132×10^{-5}	3.643×10^{-6}	6.786×10^{-7}	8.876×10^{-6}	-3.021×10^{-5}	-2.980×10^{-7}
	FEA	2.157×10^{-5}	3.534×10^{-6}	6.605×10^{-7}	8.660×10^{-6}	-3.079×10^{-5}	-3.161×10^{-7}
	Error (%)	1.16	3.08	2.74	2.49	1.88	5.72

Table 4 Comparison of intensity of constraint screw system and actuator forces of the 2PRU-UPR PM in the analytical and FEA methods

Configuration	Method	f_{11}	f_{12}	f_{1a}	f_{21}	f_{22}	f_{2a}	f_{31}	f_{32}	f_{3a}
1	Analytical	117.06	31.42	247.56	117.06	31.42	247.56	98.14	0	228.65
	FEA	117.05	31.42	247.56	117.05	31.42	247.56	98.14	0	228.65
	Error (%)	0.09	0	0	0.09	0	0	0	0	0
2	Analytical	123.34	33.83	249.12	119.88	24.97	255.12	90.22	14.48	226.39
	FEA	127.55	34.08	253.32	116.36	24.72	251.61	90.22	14.87	226.39
	Error (%)	3.30	0.73	1.66	3.03	1.01	1.40	0	2.62	0

parallel to the revolute axis, and a couple W_{3c3} on the moving platform when its gravity is ignored. There are two approaches to deal with this issues that the constraint wrench is not directly exerted on the connection point with the moving platform: one is to map the elastic deformation caused by rod gravity to the constraint wrench $\$_{3c2}$; the other is to translate the constraint wrench W_{3c2} acting on the point B_3 to the point A_3 and attach a couple W_{3c4} along x_3-axis, and satisfy $W_{3c4} = q_3 W_{3c2}$.

For the scenario 1 of the UPR limb: the compliance/stiffness matrix of the UPR limb corresponding to the kinematics-based constraint wrenches can be found in Ref. [5]. According to screw theory, the works done by the kinematics-based constraint wrenches on the twist screw $\boldsymbol{S}_{31}$ and $\boldsymbol{S}_{32}$ of the two axes of the universal joint are zero. Accordingly, the gravity-attached constrained wrenches can be obtained based on Eq. (14):

$$\begin{cases} W_{3g1} = -0.5 q_{3x} a_3, \\ W_{3g2} = -0.5 q_{3y} a_3. \end{cases} \tag{20}$$

Thus, the projection of the elastic deformation caused by the rod gravity on the kinematics-based constraint wrenches can be obtained as follows:

$$\boldsymbol{\Delta}_{3gc} = \left[\frac{q_{3z} a_3^2}{2EA} \;\; d_{3gy} + \theta_{3gx} a_3 \;\; \theta_{3x} (\boldsymbol{R}_3 \boldsymbol{e}_1 \cdot \boldsymbol{\tau}) \right], \tag{21}$$

where $d_{3gy} = \frac{W_{3g2} a_3^3}{3EI} + \frac{q_{3y} a_3^4}{8EI}$ and $\theta_{3gx} = -\frac{W_{3g2} a_3^2}{2EI} - \frac{q_{3y} a_3^3}{6EI}$ are the linear displacement deformation of the point A_3 along the y_3-axis and the angular displacement deformation along the x_3-axis caused by the rod gravity, respectively. $\boldsymbol{\tau}$ is the unit vector of the constraint couple W_{3c3}.

For the scenario 2 of the UPR limb: Due to the coupling relation between W_{3c4} and W_{3c2}, as well as the linear displacement along the y_3-axis and the angular displacement along the x_3-axis, the number of the independent kinematics-based constraint wrenches is three. Thus, the overall stiffness matrix of the mechanism without considering gravity can be expressed as follows:

$$\boldsymbol{K} = \sum_{i=1}^{2} \boldsymbol{J}_{ic} \boldsymbol{K}_{ic} \boldsymbol{J}_{ic}^{\mathrm{T}} + \boldsymbol{J'}_{3c} \boldsymbol{D}_3 \boldsymbol{K}_{3c} \boldsymbol{D}_3^{\mathrm{T}} \boldsymbol{J'}_{3c}^{\mathrm{T}}, \tag{22}$$

with

$$\boldsymbol{D}_3 = \begin{bmatrix} 1 & 0 & 0 \\ 0 & 1 & 0 \\ 0 & 0 & 1 \\ 0 & a_3 & 0 \end{bmatrix}, \tag{23}$$

where $\boldsymbol{D}_3$ is the mapping matrix from $[W_{3c1}, W_{3c2}, W_{3c3}]^{\mathrm{T}}$ to $[W_{3c1}, W_{3c2}, W_{3c3}, W_{3c4}]^{\mathrm{T}}$. The results of Eq. (22) is essentially consistent with that of Ref. [5]. Actually, the $\boldsymbol{J'}_{3c} \boldsymbol{D}_3$ in Eq. (22) of approach 2 is consistent with $\boldsymbol{J}_{3c}$ in scheme 1.

Since the coupling relation of W_{3c4} and W_{3c2}, the gravity-attached constrained wrenches are consistent with that of scheme 1. Now, the elastic deformation corresponding to

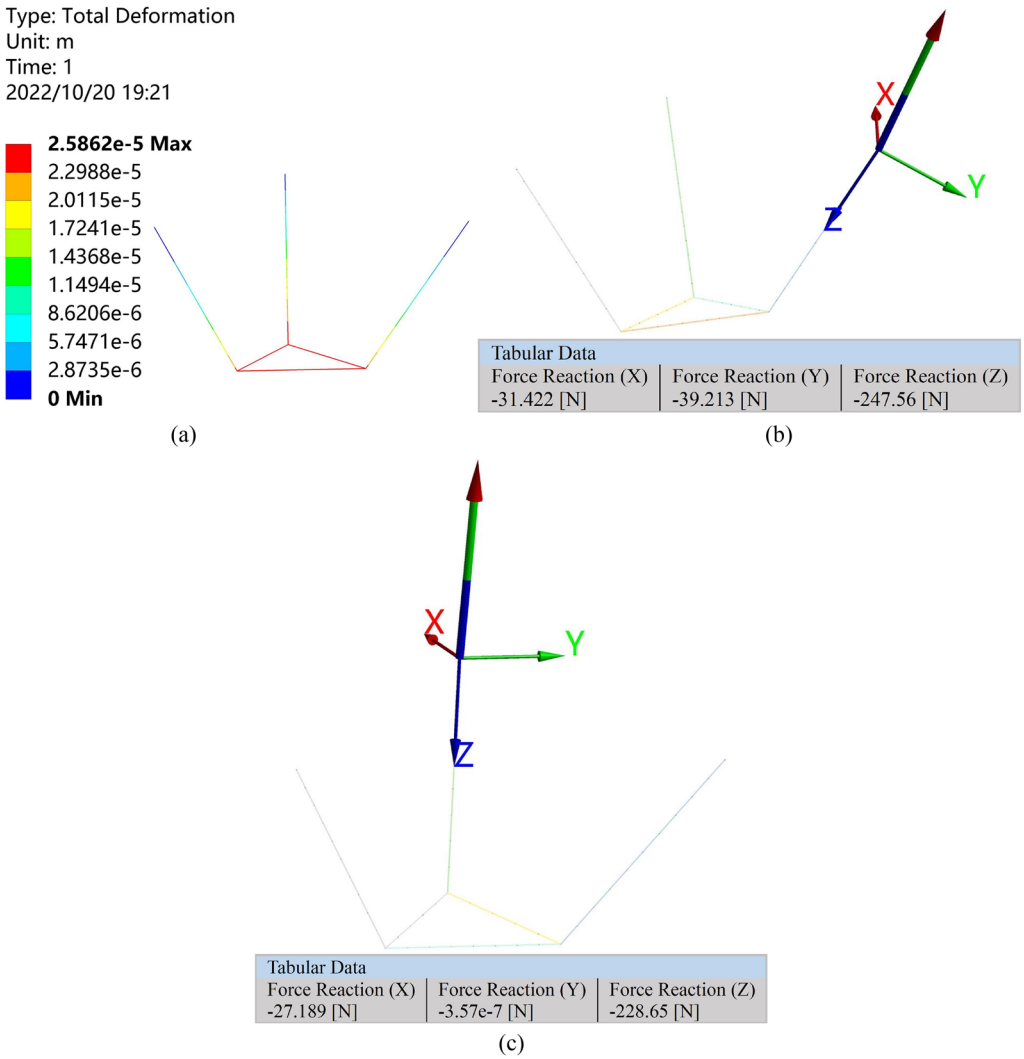

Figure 10 FEA results for the configuration 1 of the 2PRU-UPR PM: (**a**) Total deformation, (**b**) Force reaction at point B_1, (**c**) Force reaction at point B_3

the kinematics-based constraint wrenches caused by rod gravity can be established as follows:

$$\boldsymbol{\Delta}'_{3\mathrm{gc}} = \left[\frac{q_{3z}a_3^2}{2EA} \;\; d_{3\mathrm{gy}} \;\; \theta_{3x}(\boldsymbol{R}_3\boldsymbol{e}_1 \cdot \boldsymbol{\tau}) \;\; \theta_{3\mathrm{g}x}a_3 \right]. \tag{24}$$

Accordingly, the infinitesimal twist of the point o of the moving platform can be obtained by Eq. (12), herein, $\boldsymbol{J}_{ic1} = [\boldsymbol{R}_i\boldsymbol{e}_3, \boldsymbol{oA}_i \times \boldsymbol{R}_i\boldsymbol{e}_3]^{\mathrm{T}}$, $\boldsymbol{J}_{ic2} = [\boldsymbol{R}_i\boldsymbol{e}_1, \boldsymbol{oA}_i \times \boldsymbol{R}_i\boldsymbol{e}_1]^{\mathrm{T}}$, $\boldsymbol{J}_{ic3} = [0, 0, 0, \boldsymbol{\tau}]^{\mathrm{T}}$, $\boldsymbol{J}_{ig} = [\boldsymbol{R}_i\boldsymbol{e}_2, \boldsymbol{oA}_i \times \boldsymbol{R}_i\boldsymbol{e}_2]^{\mathrm{T}}$ $(i = 1, 2)$, $\boldsymbol{J}_{3c1} = [\boldsymbol{R}_3\boldsymbol{e}_3, \boldsymbol{oA}_3 \times \boldsymbol{R}_3\boldsymbol{e}_3]^{\mathrm{T}}$, $\boldsymbol{J}_{3c2} = [\boldsymbol{R}_3\boldsymbol{e}_2, \boldsymbol{oB}_3 \times \boldsymbol{R}_3\boldsymbol{e}_2]^{\mathrm{T}}$, $\boldsymbol{J}_{3c3} = [0, 0, 0, \boldsymbol{\tau}]^{\mathrm{T}}$, $\boldsymbol{J}_{3g1} = [\boldsymbol{R}_3\boldsymbol{e}_1, \boldsymbol{oA}_3 \times \boldsymbol{R}_3\boldsymbol{e}_1]^{\mathrm{T}}$, $\boldsymbol{J}_{3g2} = [\boldsymbol{R}_3\boldsymbol{e}_2, \boldsymbol{oA}_3 \times \boldsymbol{R}_3\boldsymbol{e}_2]^{\mathrm{T}}$, $\boldsymbol{W}_{\mathrm{gm}} = \left[\boldsymbol{G}_{\mathrm{m}}, \frac{1}{3}\sum_{i=1}^{3} \boldsymbol{oA}_i \times \boldsymbol{G}_{\mathrm{m}}\right]$, and $\boldsymbol{G}_{\mathrm{m}} = [0, 0, \rho A_{\mathrm{m}} hg]$, A_{m} and $h = 50$ mm are the basal area and height of the moving platform. For the approach 2: $\boldsymbol{J}'_{3c2} = [\boldsymbol{R}_3\boldsymbol{e}_2, \boldsymbol{oA}_3 \times \boldsymbol{R}_3\boldsymbol{e}_2]^{\mathrm{T}}$, $\boldsymbol{J}'_{3c4} = [0, 0, 0, \boldsymbol{R}_3\boldsymbol{e}_1]^{\mathrm{T}}$.

Similarly, the actuation force of the ith limb to balance gravity loads can be obtained through Eq. (17).

Two configurations are considered to verify the correctness of the proposed method: Configuration 1, a symmetric configuration, $z = 600$ mm, $\beta = 0$, and $\gamma = 0$; configuration 2, an asymmetric configuration, $z = 600$ mm, $\beta = 5°$, and $\gamma = -6°$. Table 3 shows the relative error of infinitesimal twist of point o of the 2PRU-UPR PM between the analytical and FEA methods with the consideration of gravity, the maximum relative angular twist error is 5.72% of that around Z-axis, the maximum relative linear twist error is 3.08% of that along Y-axis. Table 4 shows the comparison of the intensity of constraint wrenches and actuator forces of the 2PRU-UPR PM, the maximum relative error is within 3.3%. The results show the effectiveness of the kinetostatic modeling with consideration of gravity proposed in this paper.

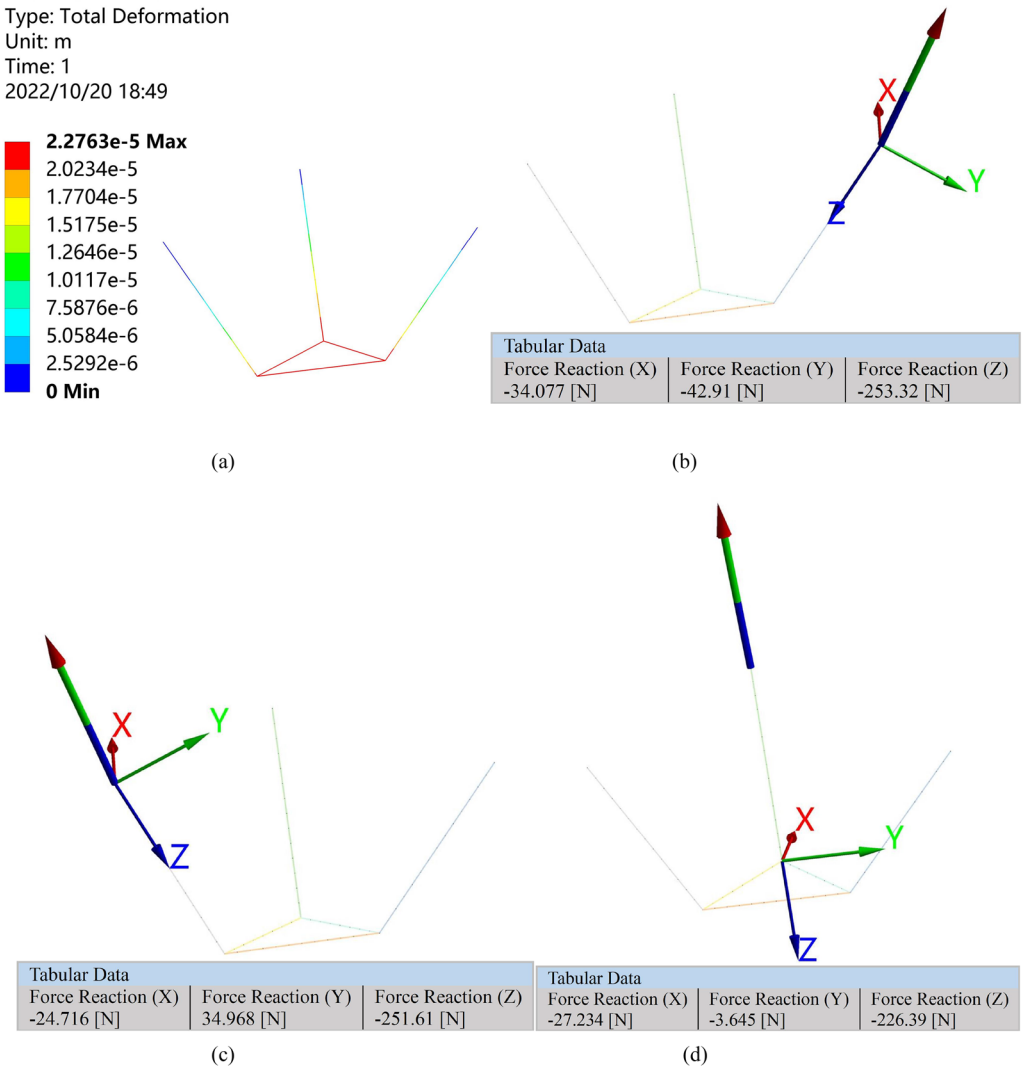

Figure 11 FEA results for the configuration 2 of the 2PRU-UPR PM: (**a**) Total deformation, (**b**) Force reaction at point B_1, (**c**) Force reaction at point B_2, (**d**) Force reaction at point B_3

Figures 10 and 11 show the FEA results of Configurations 1 and 2 of the 2PRU-UPR PM, respectively.

Figure 12 shows the infinitesimal twist of the point o of the 2PRU-UPR PM under the gravity load in the cuboid regular workspace with $-10° \leq \beta, \gamma \leq 10°$ and 300 mm $\leq z \leq$ 600 mm [5]. The maximum linear twist reaches 26 μm, the maximum angular twist reaches 0.0075°. Figure 13 shows the distribution of the actuator force of the mechanism in the regular workspace under gravity load, the additional maximum actuator force 496 N is required to equilibrium the gravity of the mechanism. The comparison analysis of two cases that include a non-overconstrained PM and an overconstrained PM shows the rationality of the proposed modeling in this work.

5 Conclusions

(1) This work proposed a kinetostatic modeling approach for PMs based on the screw theory with the consideration of gravity. Based on the dual property of the twist screw and constraint wrenches, the concept of gravity-attached constraint wrenches independent of external loads, as well as gravity-attached elastic deformation in the direction of the kinematics-based constraint wrenches were proposed. The influence of component gravity and external load on the infinitesimal twist of the end of PMs was decoupled. The proposed method is applicable to non-redundant

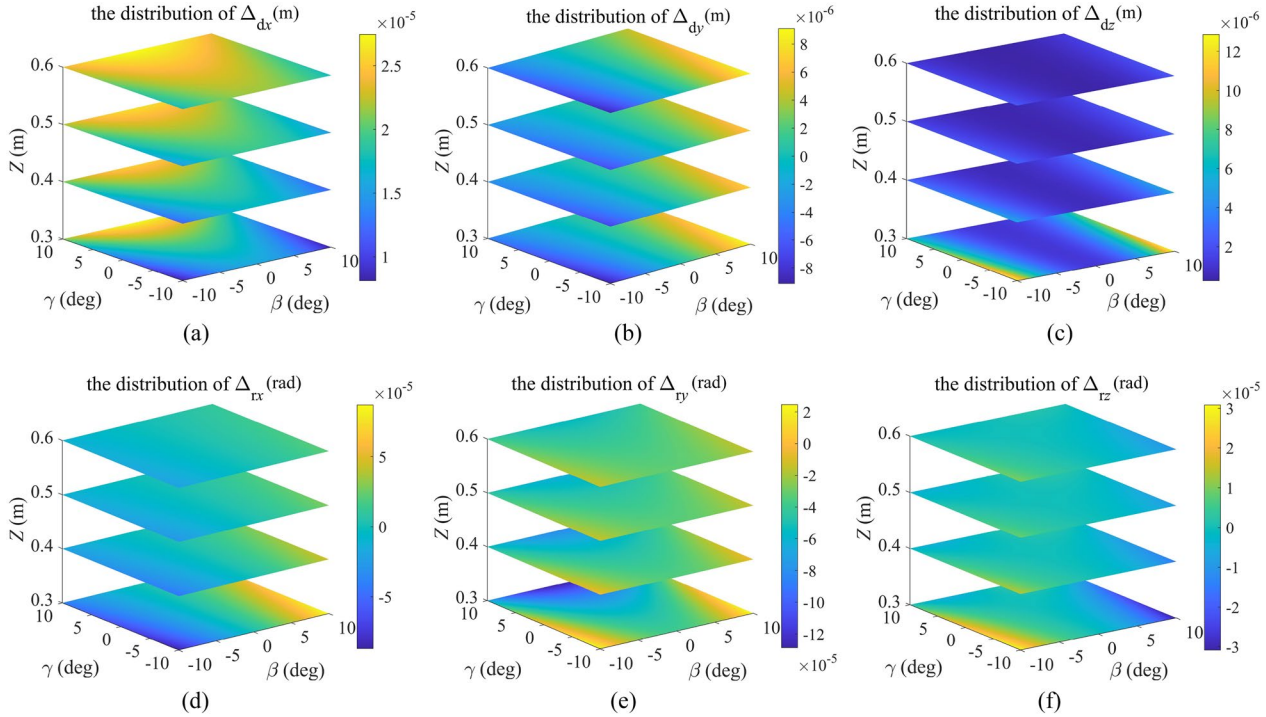

Figure 12 Infinitesimal twist of point *o* of the 2PRU-UPR PM under the influence of gravity: (**a**) Δ_{dx}, (**b**) Δ_{dy}, (**c**) Δ_{dz}, (**d**) Δ_{rx}, (**e**) Δ_{ry}, (**f**) Δ_{rz}

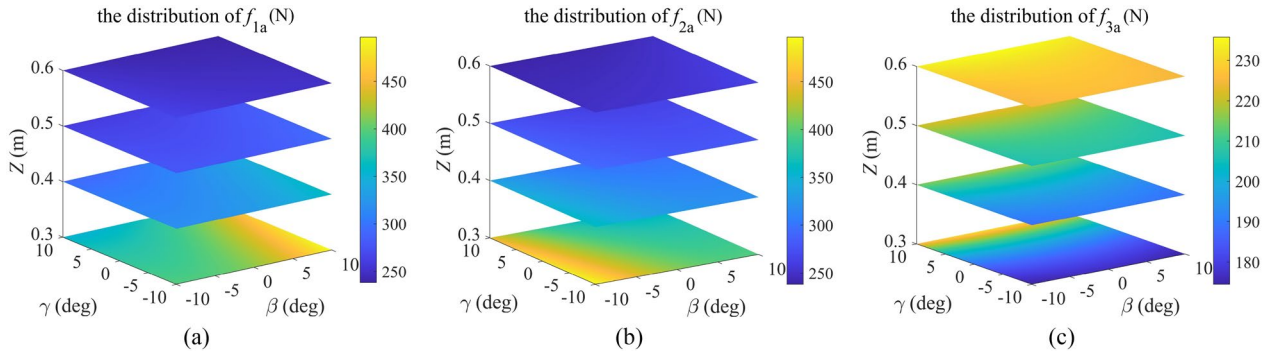

Figure 13 Actuator force of the 2PRU-UPR PM under the influence of gravity: (**a**) f_{1a}, (**b**) f_{2a}, (**c**) f_{3a}

actuated non-overconstrained and overconstrained PMs.

(2) The 3RPS PM (a non-overconstrained PM) and 2PRU-UPR PM (an overconstrained PM) were considered as two cases to implement the proposed approach. The maximum relative errors of the linear infinitesimal twist of the moving platform and the actuator force between theoretical and FEA methods for the 3RPS PM are within 0.5% and 0.2%, respectively, and that for the 2PRU-UPR PM are less than 3.08% and 1.66%, respectively. An additional actuator force of 600 N is required to balance the gravity of the 3RPS PM, and 496 N is needed in the 2PRU-UPR PM. The numerical results demonstrate the accuracy of the proposed gravity modeling, which can be considered as a gravity compensation modeling for the feedforward control of PMs. In future works, experimental research on the error compensation of gravity will be carried out to improve the pose accuracy of parallel robots.

Acknowledgements
The authors would like to thank to Pro. Qinchuan Li of Zhejiang Sci-Tech University, China, for his critical discussion and reading during manuscript preparation.

Authors' Contributions
CY contributed the conceptualization, methodology, numerical simulation, and original draft of the paper. FH contributed the visualization and supervision of original data, figures, and code of the paper. WY contributed the simulation work, review and editing of the paper. QC contributed the conceptualization and revised the paper. All authors read and approved the final manuscript.

Authors' Information
Chao Yang, born in 1982, is currently a Lecturer at *College of Mechanical and Electrical Engineering, Jiaxing University, China*. He received the B.S. degree from *Zhengzhou University of Light Industry, China*, in 2005, the M.S. degree in engineering mechanics from *Dalian University of Technology, China*, in 2009, and a Ph.D. degree in mechanical engineering from *Zhejiang Sci-Tech University, China*, in 2019. His research interests include kinematics, stiffness, dynamics, and multi-objective optimization of parallel manipulators.
Fengli Huang, born in 1976, is currently a professor at *College of Mechanical and Electrical Engineering, Jiaxing University, China*. He received his B.S. degree in thermal engineering from *Kunming University of Science and Technology, China*, in 2000, the M.S. degree in mechanical engineering from *Zhejiang University of Technology, China*, in 2005, and a Ph.D. degree in mechanical engineering from *Tongji University, China*, in 2010.
Wei Ye, born in 1988, is currently an associate professor at *Faculty of Mechanical Engineering & Automation, Zhejiang Sci-Tech University, China*. He received his B.S. and Ph.D. degrees in mechanical engineering from *Beijing Jiaotong University, China*, in 2010 and 2016, respectively. His research interests include mechanism theory of parallel manipulators and application.
Qiaohong Chen, born in 1976, is currently a professor at *Zhejiang Sci-Tech University, China*. She received her Ph.D. degree in mechanical engineering from *Zhejiang Sci-Tech University, China*, in 2012. Her research interests include kinematics and computer-aided design of parallel manipulator, and pattern recognition.

Funding
Supported by National Natural Science Foundation of China (Grant No. 52275036) and Key Research and Development Project of Jiaxing Science and Technology Bureau of China (Grant No. 2022BZ10004).

Availability of Data and Materials
The corresponding author can provide MATLAB and ANSYS files to support the work.

Declarations

Competing Interests
The authors declare no competing financial interests.

Received: 14 December 2022 Revised: 6 November 2023 Accepted: 12 November 2023
Published online: 18 December 2023

References

[1] M J Thomas, M L Joy, A P Sudheer. Kinematic and dynamic analysis of a 3-prus spatial parallel manipulator. *Chinese Journal of Mechanical Engineering*, 2020, 33: 13. https://doi.org/10.1186/S10033-020-0433-8
[2] A Klimchik, D Chablat, A Pashkevich. Stiffness modeling for perfect and non-perfect parallel manipulators under internal and external loadings. *Mechanism and Machine Theory*, 2014, 79: 1-28. https://doi.org/10.1016/j.mechmachtheory.2014.04.002
[3] C Yang, W Ye, Q C Li. Review of the performance optimization of parallel manipulators. *Mechanism and Machine Theory*, 2022, 170: 104725.
[4] W K Yoon, T Suehiro, Y Tsumaki, et al. Stiffness analysis and design of a compact modified Delta parallel mechanism. *Robotica*, 2004, 22: 463-475. https://doi.org/10.1017/S0263574704000050
[5] C Yang, Q C Li, Q H Chen. Analytical elastostatic stiffness modeling of parallel manipulators considering the compliance of the link and joint. *Applied Mathematical Modelling*, 2020, 78: 322-349. https://doi.org/10.1016/j.apm.2019.10.024.
[6] D Deblaise, X Hernot, P Maurine. A systematic analytical method for PKM stiffness matrix calculation. *Proceedings of the 2006 IEEE International Conference on Robotics and Automation (ICRA)*, Orlando, Florida, May 2006: 4213-4219.
[7] A Klimchik, A Pashkevich, D Chablat. Fundamentals of manipulator stiffness modeling using matrix structural analysis. *Mechanism and Machine Theory*, 2019, 133: 365-394. https://doi.org/10.1016/J.MECHMACHTHEORY.2018.11.023.
[8] A Pashkevich, D Chablat, P Wenger. Stiffness analysis of overconstrained parallel manipulators. *Mechanism and Machine Theory*, 2009, 44(5): 966-982. https://doi.org/10.1016/j.mechmachtheory.2008.05.017.
[9] C Zhao, H Guo, D Zhang, et al. Stiffness modeling of n(3RRIS) reconfigurable series-parallel manipulators by combining virtual joint method and matrix structural analysis. *Mechanism and Machine Theory*, 2020, 152: 103960. https://doi.org/10.1016/j.mechmachtheory.2020.103960.
[10] B Hu, Z Huang. Kinetostatic model of overconstrained lower mobility parallel manipulators. *Nonlinear Dynamics*, 2016, 86(1): 309-322. https://doi.org/10.1007/s11071-016-2890-2.
[11] Y D Xu, W Liu, J T Yao, et al. A method for force analysis of the overconstrained lower mobility parallel mechanism. *Mechanism and Machine Theory*, 2015, 88: 31-48. https://doi.org/10.1016/j.mechmachtheory.2015.01.004.
[12] Y D Xu, J T Yao, Y Zhao. Internal forces analysis of the active overconstrained parallel manipulators. *International Journal of Robotics Automation*, 2015, 30(5): 511-518. https://doi.org/10.2316/Journal.206.2015.5.206-4422.
[13] S J Yan, S K Ong, A Y C Nee. Stiffness analysis of parallelogram-type parallel manipulators using a strain energy method. *Robotics and Computer-Integrated Manufacturing*, 2016, 37: 13-22. https://doi.org/10.1016/j.rcim.2015.05.004.
[14] A Rezaei, A Akbarzadeh, M R Akbarzadeh-T. An investigation on stiffness of a 3-PSP spatial parallel mechanism with flexible moving platform using invariant form, *Mechanism and Machine Theory*, 2012, 51: 195-216. https://doi.org/10.1016/j.mechmachtheory.2011.11.011.
[15] C Yang, Q C Li, Q H Chen, et al. Elastostatic stiffness modeling of overconstrained parallel manipulators. *Mechanism and Machine Theory*, 2018, 122: 58-74. https://doi.org/10.1016/j.mechmachtheory.2017.12.011.
[16] B B Lian, T Sun, Y M Song, et al. Stiffness analysis and experiment of a novel 5-DoF parallel kinematic machine considering gravitational effects. *International Journal of Machine Tools & Manufacture*, 2015, 95: 82-96. https://doi.org/10.1016/j.ijmachtools.2015.04.012.
[17] T Sun, B B Lian, Y M Song. Stiffness analysis of a 2-DoF over-constrained RPM with an articulated traveling platform, *Mechanism and Machine Theory*, 2016, 96: 165-178. https://doi.org/10.1016/j.mechmachtheory.2015.09.008.
[18] J Jesus Cervantes-Sanchez, J M Rico-Martinez, S Pacheco-Gutierrez, et al. Static analysis of spatial parallel manipulators by means of the principle of virtual work. *Robotics and Computer-Integrated Manufacturing*, 2012, 28(3): 385-401. https://doi.org/10.1016/j.rcim.2011.11.002.
[19] M Wang, H Liu, T Huang, et al. Compliance analysis of a 3-SPR parallel mechanism with consideration of gravity. *Mechanism and Machine Theory*, 2015, 84: 99-112. https://doi.org/10.1016/j.mechmachtheory.2014.10.002.
[20] W A Cao, H Ding, W Zhu. Stiffness modeling of overconstrained parallel mechanisms under considering gravity and external payloads. *Mechanism and Machine Theory*, 2019, 135: 1-16. https://doi.org/10.1016/j.mechmachtheory.2018.12.031.
[21] B Mei, F G Xie, X J Liu, et al. Elasto-geometrical error modeling and compensation of a five-axis parallel machining robot. *Precision Engineering*, 2021, 69: 48-61. https://doi.org/10.1016/j.precisioneng.2021.01.007.
[22] C Zhao, Z Chen, J Song, et al. Deformation analysis of a novel 3-DOF parallel spindle head in gravitational field. *Mechanism and Machine Theory*, 2020, 154: 104036. https://doi.org/10.1016/j.mechmachtheory.2020.104036.
[23] A Taherifar, H Salarieh, A Alasty, et al. Inverse and forward dynamics of N-3RPS manipulator with lockable joints. *Robotica*, 2016, 34(6): 1383-1402. https://doi.org/10.1017/S0263574714002355.
[24] L M Xu, Q C Li, N B Zhang, et al. Mobility, kinematic analysis, and dimensional optimization of new three-degrees-of-freedom parallel

manipulator with actuation redundancy. *Journal of Mechanisms and Robotics*, 2017, 9(4): 041008.

[25] C Yang, Q H Chen, J H Tong, et al. Elastostatic stiffness analysis of a 2pur-psr overconstrained parallel mechanism. *International Journal of Precision Engineering and Manufacturing*, 2019, 20(4): 569-581. https://doi.org/10.1007/s12541-019-00077-1.